Stochastic Collective Movement of Cells and Fingering Morphology: No Maverick Cells

Gaddiel Yonathan Ouaknin* and Pinhas Zvi Bar-Yoseph
Computational Biomechanics Laboratory, Faculty of Mechanical Engineering, Technion, Israel Institute of Technology, Haifa, Israel

ABSTRACT The classical approach to model collective biological cell movement is through coupled nonlinear reaction-diffusion equations for biological cells and diffusive chemicals that interact with the biological cells. This approach takes into account the diffusion of cells, proliferation, death of cells, and chemotaxis. Whereas the classical approach has many advantages, it fails to consider many factors that affect multicell movement. In this work, a multiscale approach, the Glazier-Graner-Hogeweg model, is used. This model is implemented for biological cells coupled with the finite element method for a diffusive chemical. The Glazier-Graner-Hogeweg model takes the biological cell state as discrete and allows it to include cohesive forces between biological cells, deformation of cells, following the path of a single cell, and stochastic behavior of the cells. Where the continuity of the tissue at the epidermis is violated, biological cells regenerate skin to heal the wound. We assume that the cells secrete a diffusive chemical when they feel a wounded region and that the cells are attracted by the chemical they release (chemotaxis). Under certain parameters, the front encounters a fingering morphology, and two fronts progressing against each other are attracted and correlated. Cell flow exhibits interesting patterns, and a drift effect on the chemical may influence the cells' motion. The effects of a polarized substrate are also discussed.

INTRODUCTION

Collective migration of cells has an important place in many physiological processes, such as metastasis, morphogenesis, bone remodeling, and wound and fracture healing. Cell movement can be stimulated by different mechanisms, such as chemotaxis (1), durotaxis (2), galvanotaxis, thermotaxis, and haptotaxis, as well as polarization of the extracellular matrix, which can direct the cell motion (3). A single biological cell moves with its internal mechanisms of regulation of the proteins actin and myosin. Mathematical models of a single cell have been developed, and some understanding has been reached (e.g., (4,5) and references therein). Despite the complex biophysics of cell locomotion at the cellular level, the multicell movement is coordinated between the different cells that constitute the tissue. Via chemical signals and strong cadherin contacts, cells are able to move in a collective way. Collective cell movement leads to patterns that cannot be deduced by studying single cell movement only.

Wound healing, the body's response when epidermal tissue is removed from the skin, is a complex and dynamic process of restoring cellular structures and tissue layers. Cells close to the wound send signals, start to move, and proliferate to contract the wound. In trying to understand how the different biological factors affect collective movement and especially wound healing, many biological experiments have been carried out. In wound healing, many biochemical cascades of signals occur; thus, it is almost impossible to decouple all the effects on each other. In each experiment, attempts are made to isolate another factor and to decouple it from the others.

In one study, Poujade et al. (6) used a novel experimental approach to simulate wound healing. Instead of the classical wound scratch assay, they used an original approach in which a virgin surface is presented to a confluent epithelium of Madin-Darby canine kidney cells with no damage to the cells. In their experiment, the cells at the border remain intact, allowing uncoupling of the effect of damaged cells to the process. The cells start moving to the unwounded region dragged by leader cells. The front exhibits a fingering morphology and a very complex flow of cells is observed (6,7).

Nikolie et al. (8) also investigated the role of boundary conditions during epithelial wound healing. They show that injury triggers faster cell motion than free surface alone. In addition, in this case (8), a fingering morphology is clearly seen, and the collective cell movement shows high coordination.

In another study, Farooqui and Fenteany (9), using the same type of cells, investigated wound healing and focused on the differences in velocity of the different cells inside the undamaged tissue as a function of their initial distance from the wound front. Additionally, Grasso et al. (10) investigated wound geometry, wound size, and extracellular matrix (ECM) roles in the healing of bovine corneal endothelial cells in culture. In both of these cases as well, a fingering morphology clearly appears later in Figs. 9 and 10. Bindschadler and McGrath (11) investigated L1 fibroblasts with the scratch-wound assay and found that sheet migration can be explained by a simple single-cell movement model and does not require intercellular interaction.

The exact biophysical mechanism in wound healing is still unclear. Mathematical models to quantify the multicell

Submitted December 17, 2008, and accepted for publication May 26, 2009.

*Correspondence: gaddy@tx.technion.ac.il

Editor: Herbert Levine.

0006-3495/09/10/1811/11 $2.00

doi: 10.1016/j.bpj.2009.05.064

migration in wound healing can contribute to a better understanding of wound healing. Such insights can be of great concern for clinical purposes. For example, they can aid in the development of drugs designed to efficiently contract a wound or for aesthetic surgical purposes.

Many theoretical and numerical studies have already been carried out to model the collective cell movement (12). Usually these models assume a continuous distribution of the chemicals and the cells, and they use nonlinear coupled partial differential equations. These models include reaction, diffusion, chemotaxis, proliferation, decay, and secretion of chemicals by cells. The change in density of cells from a certain type is due to cell migration, mitotic generation, transition to other types and transition from other types, and motion up or down of chemical gradients. In diffusive chemicals, the change in density is due to diffusion, production of chemicals by cells, and reaction between other chemicals, which can be a gain or a loss depending on the other diffusive chemical concentrations.

The Sherratt and Murray (13) model uses Eqs. 1 and 2 to describe epidermal wound healing:

$$\underbrace{\frac{\partial n}{\partial t}}_{\text{Rate of increase of cell density}} = \underbrace{D_n \nabla^2 n}_{\text{Cell migration}} + \underbrace{s(c) n \left(1 - \frac{n}{n_0}\right)}_{\text{Mitotic generation and natural loss}}, \quad (1)$$

$$\underbrace{\frac{\partial c}{\partial t}}_{\text{Rate of increase of chemical concentration}} = \underbrace{D \nabla^2 c}_{\text{Diffusion}} + \underbrace{f(n)}_{\text{Production by cells}} - \underbrace{\gamma c}_{\text{Decay of active chemical}}. \quad (2)$$

Sherratt and Murray assume migration with a constant diffusion coefficient, and mitosis controlled by a diffusive chemical. The interaction of the chemical with its surroundings is expressed by a single term (the last term in Eq. 2). They solve these two coupled nonlinear equations using a finite difference scheme in one dimension for a radial geometry and get $n(r)$, and $c(r)$. This model was extended by Dale et al. (14) to model corneal epithelium wound healing in which they take the diffusion coefficient to be dependent on the diffusive chemical. Maini et al. (15,16) solved the Fisher equation in one dimension and fit the simulation parameters using experimental data. They received a constant front speed during the wound healing with this model. Cai et al. (17) extended the one-dimensional Fisher equation by introducing diffusivity that depends on the cell concentration:

$$\underbrace{\frac{\partial n}{\partial t}}_{\text{Rate of increase of cell density}} = \underbrace{D_0 \frac{\partial}{\partial x}\left(D(n)\frac{\partial n}{\partial x}\right)}_{\text{Cell migration}} + \underbrace{\alpha n \times \left(1 - \frac{n}{n_0}\right)}_{\text{Mitotic generation and natural loss}}, \quad (3)$$

$$D(n) = \frac{n}{A + n}. \quad (4)$$

Cai et al. then used Eq. 3 to derive a master equation to include stochastic effects and single cell tracking. The advantage of this last model is that it permits a multiscale approach.

The continuous models of collective migration processes cannot simply take into account the adhesion energy between cells, the elastic energy of the cells, and the stochastic behavior of the system, and therefore they cannot follow the path of individual cells. To take the adhesion energy, deformation energy, and stochastic behavior of the system into consideration and to track cell paths, we use the well-known Glazier-Graner-Hogeweg (GGH) model (18,19) to model collective movement of cells in wound healing.

To make allowance for the adhesion between the cells as a key factor of the biological process, Graner and Glazier (18) used the Potts model from statistical mechanics and simulated the arrangement of cells with different adhesion constants. Since cells respond to chemical signals and they themselves secrete chemicals, Savill and Hogeweg (19) coupled the Potts model to a continuum reaction-diffusion equation for a diffusive chemical to add chemotaxis and secretion of chemicals by cells. They also further extended it by adding an ordinary differential equation that regulates the cell's response to chemicals, and added barrier energy to cell movement. Many studies on collective cell movement succeeded using this method.

Using the GGH model, Turner and Sherratt (20) investigated the fingering morphology in tumor invasion. They extended the model and added the possibility of cell proliferation via a probability function that depends on biological parameters. Popalawski et al. (21) also used the GGH model for biofilms. In recent years, some work has been done to bridge between the parameter values of the GGH model and those of the continuum model. Moreover, Ouchia et al. (22) systematically investigated the cell diffusion coefficient's dependence on the different GGH parameters using a computer simulation approach. Turner et al. (23) developed a master equation for a one-dimensional cell and derived from it a diffusion equation for the cells as a function of the GGH parameters. Alber et al. (24) developed a master equation for a one-dimensional cell with chemotactic interaction with an external chemical and obtained a Fokker-Plank equation for the cells. Alber et al. (25) extended this to multicell behavior and two-dimensional cells. Implementation details and strategies for how to develop a GGH program were recently published (26,27).

In this study, we take this model one step further to model wound healing and assume that the secretion of cells depends on the local cell density. We investigate the front morphology, front-front interaction, and cell flow; furthermore, we investigate the addition of a drift to the diffusion equation of the chemical, substrate polarization effects. Moreover, we take advantage of the GGH model to investigate cell dynamics at the cellular level and to track the cell path.

This article is organized as follows: first, the mathematical model is described; then, the fingering morphology with

a chemotaxis mechanism is presented. The interaction between two strips of cells and stochastic cell flow are then discussed. Next, the effect of adding a drift to the chemical is explained; and finally, the effect of a polarized substrate is described.

THE COMPUTATIONAL MODEL

Living cells are complex bodies that can sense mechanical forces and convert them into biological responses. Similarly, biological and biochemical signals are known to influence the abilities of cells to sense, generate, and bear mechanical forces (28).

In the model presented below, several phenomena are taken into account: the adhesive forces between biological cells; the resistance of the biological cells to deformation; and the attraction of biological cells to chemicals or biological materials. It is further assumed that biological cells secrete chemicals. Diffusion, reaction, and a source load coming from the secretion of the biological cells are also taken into account as part of the chemical dynamics. Cell dynamics is introduced via an energetic approach.

The physical core of the method is to use the energy Boltzmann distribution for a system in thermal equilibrium with a heat bath (29) and to simulate the dynamics with the Monte Carlo Hasting Metropolis algorithm (30) assuming dissipative behavior of the biological cells. The domain is discretized into elements, and each element contains a biological cell or extracellular matrix (ECM), where each biological cell has a different index,

$$[1 \le X(e) \le N_c + 1,\ e = 1, 2, \ldots . N_{el}], \tag{5}$$

where $\vec{X} = (X(1), X(2), \ldots, X(N_{el}))$ is the biological cells' state; e is the element; N_c is the number of living cells; N_{el} is the number of elements; and $X(e)$ is the cell that lives in element e. If $X(e) = N_c + 1$, at element e, there is no biological cell but the ECM. A generalized cell is a collection of connected elements with the same index value. The number of elements in a cell is its area, and the number of elements on its boundary (interfaces with other indices) is its perimeter. In two dimensions, in the second nearest-neighbor approximation, each element has eight neighbors.

In our case, the energy of the system is composed of three main components: adhesion, elastic, and chemical energy. To model other physical constraints, additional terms can be added to the energy (31).

The adhesion energy is the energy between a cell and its surroundings. The interaction is also with the ECM and can be represented using an adhesion matrix,

$$\overleftrightarrow{J} = \begin{bmatrix} J_{cc} & J_{cm} \\ J_{cm} & J_{mm} \end{bmatrix}, \tag{6}$$

where c designates the cell type and m, the ECM type; J_{cc} represents the cell-cell adhesion interaction; J_{cm} the cell-ECM adhesion interaction; and J_{mm} the ECM-ECM adhesion interaction, which is usually taken as zero, as

$$H_{adhesion} = \frac{1}{2}\sum_{e=1}^{N_{el}} \sum_{n=1}^{8} J_{type(X(e)),type(X(e_n))} \times \left(1 - \delta_{X(e),X(e_n)}\right), \tag{7}$$

where e_n is the n^{th} neighbor of e. Both positive and negative surface energies can be used where negative surface energies between cells are more physical, since the biological cells are cohesive (22). Adhesion energy mimics the physical behavior of the cadherin proteins at the membrane. Real biological cells may not have a constant protein density at the membrane, as they may diffuse there or encounter chemical reactions. In this model, adhesion energy is taken as a constant.

The deformation energy quantifies the energy needed to deform the membrane. It calculates the deviation of the cell from its target area and its target perimeter,

$$H_{deformation} = \sum_{j=1}^{N_c(t)} \lambda_1 \times \left(A_j - A_{target}(j)\right)^2 + \lambda_2 \times \left(Per_j - Per_{target}(j)\right)^2, \tag{8}$$

where A_j is the area of cell j; Per_j is the perimeter of cell j; $\lambda^{1,2}$ are the deformation parameters; $A_{target}(j)$ is the target area of cell j; and $Per_{target}(j)$ is the target perimeter of cell j. In the deformation energy, we include a parameter that quantifies the deviation of the perimeter from its target perimeter to prevent the cells from splitting and to control the cell shape. This energy, in combination with the temperature, controls the fluctuations of the membrane. Popalawski (32) proposed deformation energy more consistent with classical elasticity. In fact, this term can be related to the constitutive equation of a material. The curvature of the surface is not taken explicitly as in other continuous models (33) in deformation energy; however, the ratio between the area perimeter and target perimeter controls the shape of the biological cells.

The chemical energy depends on the chemical's concentration (c) and the cells' chemical potential (μ). The gradient of the chemical concentration is the driving force of chemotaxis, where the cell velocity is proportional to the chemical gradient $\vec{v}\infty \propto \vec{\nabla} c$,

$$H_{chemical} = \sum_{j=1}^{N_c} \mu_j \times \sum_{i=1}^{A_j} c(e_i), \tag{9}$$

where e^i is the i^{th} element of cell j.

The dynamics is simulated with the Monte Carlo Hasting Metropolis method (30), which ensures detailed balance. At each iteration, an element R1 is chosen randomly. Then, one of its eight neighbors, R2, is also chosen randomly. If $X(R1) = X(R2)$, the random selection is repeated. When we get an $X(R1)$ that differs from $X(R2)$, we change the value of $X(R1)$ in $X(R2)$ and calculate which change in energy it may cause, as

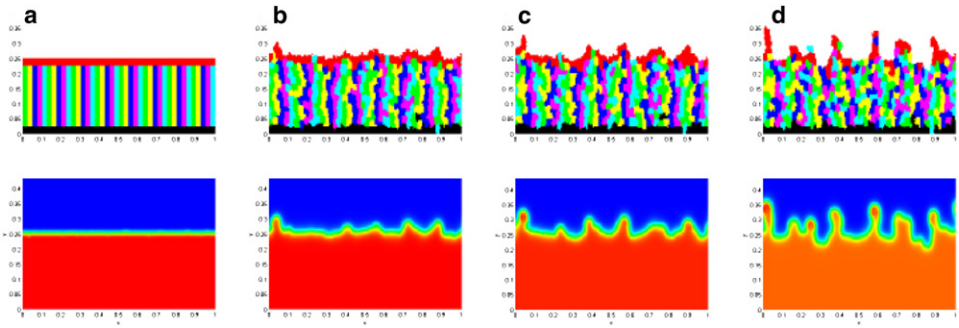

FIGURE 1 Sequence of images of one strip of biological cells moving forward. (*First row*) Cell state. (*Second row*) Chemical field. $D = 0.005$; $\gamma = 50$. The fingering morphology is well seen in both the cell state and the chemical state. (*a*) 0 MCS, (*b*) 600 MCS, (*c*) 900 MCS, and (*d*) 1800 MCS.

$$\Delta H = \Delta H_{\text{adhesion}} + \Delta H_{\text{deformation}} + \Delta H_{\text{chemical}}. \quad (10)$$

Not all the energy is calculated at each of the iterations, but just the reversal between elements R1 and R2. Then, the attempted change is accepted with probability,

$$P_{\text{acceptance}}(\Delta H) = \begin{cases} 1 \text{ if } \Delta H + H_0 < 0 \\ e^{\frac{-\Delta H + H_0}{T}} \text{ if } \Delta H + H_0 \geq 0 \end{cases}, \quad (11)$$

where H_0 is threshold energy due to the dissipation when creating and breaking membrane contacts (22).The threshold energy is a parameter of the model and is usually chosen in the same size of order of the other energies. The threshold energy reduces the probability of changes in the cell state since it increases the energy.

The temperature T used in the GGH model is not the temperature of a reservoir, but rather a temperature that controls the fluctuations of the biological membrane. In fact, it can be seen as an internal energy of the biological cell that converts ATP into mechanical energy. In fact, what is important in the GGH parameters is not their absolute value, but rather their difference divided by the temperature: $(\Delta H + H_0)/T$. A value of λ_1/T that is too low will allow the cell to shrink, whereas a value of λ_2/T that is too low will allow the cells to split. Values of λ_1/T and λ_2/T that are too high will lock the system around metastable states. The deformation parameters with the temperature scale controls the fluctuations of the membrane, whereas the chemical potential divided by the temperature controls the chemical force applied on the cells. The cell state is coupled to a diffusive chemical field that is simulated with a reaction-diffusion equation,

$$\begin{bmatrix} c_t = D\left(c_{xx} + c_{yy}\right) - \gamma c + f(\vec{X}) \text{ on } (0, L_x) \times \left(0, L_y\right) \\ c(0,x,y) = \begin{cases} 1 \text{ if occupied by a cell,} \\ 0 \text{ else} \end{cases} \\ \text{(Initial conditions)} \\ \dfrac{\partial c}{\partial y} = 0 \text{ on } y = 0, y = L_y \\ \text{(No flux boundary conditions)} \\ c(x = 0) = c(c = L_x), \dfrac{\partial c}{\partial x}|_{x=0} = \dfrac{\partial c}{\partial x}|_{x=L_x} \\ \text{(Periodic boundary conditions)} \end{bmatrix}, \quad (12)$$

where c is the concentration of the chemical, D is the diffusion coefficient of the chemical, γ is the decay rate of the chemical, and $\vec{X}$ is the biological cells' state. The external source term $f(\vec{X})$ is a diffusible chemical secreted by the biological cells. Each cell secretes a diffusive chemical as a function of its local density. The local density is inversely proportional to the noncontact cell-cell, and we assume the cells at the front secrete a chemical at their interface with the wounded region. We assume that when cells sense a low local density, they are highly active, as in the literature (12–14), and they secrete chemicals or biological products. In turn, these chemicals may attract other cells, such as in the literature (34,35). When they are surrounded, they exhibit regular behavior, and they secrete chemicals simply to overcome the degradation and no more: no maverick cells. The diffusion equation of the diffusive chemical is solved with the finite element method in space and finite difference in time.

The values used for the decay rate and the diffusion coefficient are normalized. The space unit is the horizontal length of the simulated domain. One Monte Carlo Step (MCS) is defined to be the number of elements times the number of iterations of the Metropolis algorithm.

RESULTS AND DISCUSSION

In all the simulation results presented below, we assume the cells adhere more strongly to other cells than to the ECM ($J_{cc} < J_{cm}$). Additionally, we assume there is chemotaxis and secretion of a diffusive chemical by the epithelial cells when they sense a wounded region in their surroundings. For all simulations, the GGH parameters are:

$$\lambda_1 = 1,\ \lambda_2 = 2,\ J_{cc} = -1.6,\ J_{cm} = 0.8,\ \mu = -20,$$
$$H_0 = 0.4,\ T = 10,\ A_{\text{target}} = 5 \times 5 = 25,\ P_{\text{target}} = 20.$$

Fingering morphology with chemotaxis mechanism

First, the process is decoupled from proliferation. This mechanism assumes the secretion to be a function of the cell's local density. The fingering generation can be well understood: at

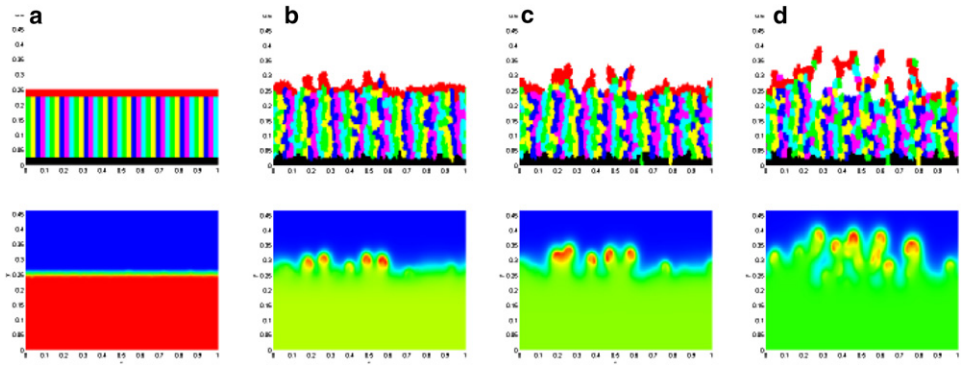

FIGURE 2 Sequence of images of one strip of biological cells moving forward. (*First row*) Cell state. (*Second row*) Chemical field. $D = 0.005$; $\gamma = 10$. The fingering morphology is well seen also in this case in both the cell state and the chemical state. (*a*) 0 MCS, (*b*) 600 MCS, (*c*) 900 MCS, and (*d*) 1800 MCS.

a specific time, some cells sense low local density, which leads to a cascade of chemical signals resulting in a release of chemicals to the wounded region. Then, to reduce their chemical energy, these cells at the front go to this region of high chemical concentration, dragging the cells of the submarginal layers and their neighbors in the same row after them. When they get to this region, they sense lower local density and then secrete even more chemicals, and so on.

In the simulations, one strip of cells with no flux boundary condition on the y axis and periodic boundary condition on the x axis is simulated using two different decay rates (see Figs. 1 and 2). To monitor the internal cell dynamics, we color the first and last row in red and black, and the columns with other colors.

A look at the field of concentration of the diffusive chemical for a constant $y = 0.35$ (Fig. 3 *a*) and a constant $x = 0.45$ (Fig. 3 *b*) clearly illustrates the fingering morphology. At $x = 0.45$, $t = 1800$ MCS (Fig. 3 *b*) between $y = 0.2$ and $y = 0.3$, and c decreases since there are no biological cells. From $y = 0.3$ to $y = 0.4$, c increases to almost two times its equilibrium value, and the cells in this region sense a low local density. They secrete enough chemical to multiply c by almost 2. Then the cells migrate to this region of high concentration to decrease their chemical energy. When they get to this region of high concentration, they secrete even more and so on. The decay rate influences the front morphology. For $\gamma = 50$, the fingers are sharper than when $\gamma = 10$. The secreted chemical in the case of $\gamma = 50$ decays too fast for the fingers to develop on its sides, and the cells just advance forward. Where $\gamma = 10$, the cells have enough time to spread to the sides.

Mean culture progression is an important subject of investigation. Poujade et al. (6) observe a linear increase of the velocity, whereas in Murray (12), Sherratt and Murray (13), Dale et al. (14), Maini et al. (15,16), and Cai et al. (17), a constant velocity is assumed, and in Farooqui and Fenteany (9) and Grasso et al. (10), the regime of the front progression is not clear. In these studies, the advancing front was measured with proliferation. In this study, the mean cell displacements are calculated in the x and y directions as a function of time for different initial rows (see Fig. 4) for the simulation shown in Fig. 2, which lacks proliferation. Effectively, on average the velocity increases with y. In the first-order, the cells perform a random motion in two dimensions, with a drift term in the y direction as a function of y,

$$d\vec{x}_i = \vec{v}_i(y,t)dt + \vec{\sigma}_i dW, \tag{13}$$

for the i^{th} cell, where dW is the increment of a random motion and $\vec{\sigma}_i$ is the random component of the displacement of the i^{th} cell (36), and the velocity is due both to chemotaxis and cell-cell adhesion interaction. These results are in accordance with the experiments of Farooqui and Fenteany (9), which show that the rate of migration is inversely proportional to the initial distance from the margin. In addition, note that a biological cell that starts at the front does not necessarily stay there but may migrate back as complex cells flow occurs (Figs. 1, 2, and later in Fig. 11). This will be discussed in the section on stochastic cell flow.

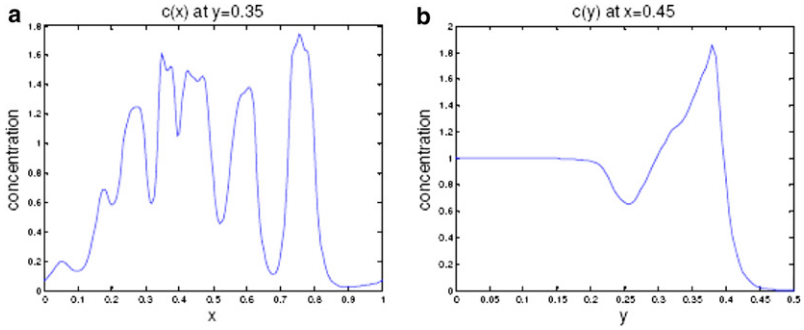

FIGURE 3 (*a*) $c(x)$ for $y = 0.35$: concentration of the chemical as function of x at the front. (*b*) $c(y)$ for $x = 0.45$: concentration of the chemical for a constant x, $t = 1800$ MCS. $D = 0.005$; $\gamma = 10$.

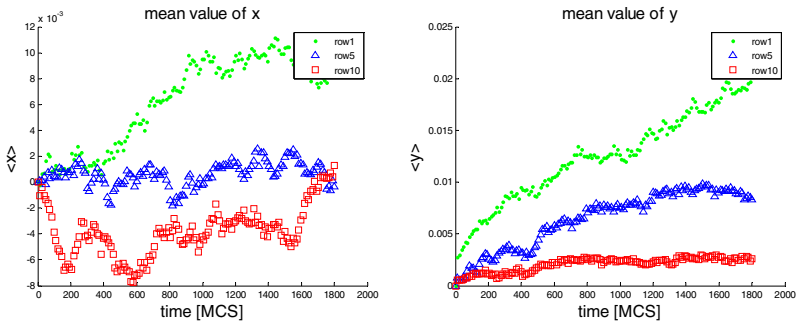

FIGURE 4 Displacement for different initial rows (*left*) $\langle x \rangle$ versus time: displacement parallel to the front; and (*right*) $\langle y \rangle$ versus time: displacement perpendicular to the front. $D = 0.005$; $\gamma = 50$.

Fig. 5 shows the progression of four independent fingers in the simulation shown in Fig. 1. Leader cells at the first order thus have a constant velocity in the y direction (perpendicular to the wound edge) added to a random motion in two dimensions,

$$d\vec{x} = v_y \hat{y} dt + \vec{\sigma} dW, \tag{14}$$

for leaders' cells.

Similar qualitative behavior is observed in the experiments of Poujade et al. (6). There as well, the leader cells progress much faster than the other cells at a constant velocity.

The influence of D and γ on the front morphology is systematically investigated. Fig. 6 shows the fingering morphology dependence on the decay rate γ and the diffusion coefficient D. For $\gamma = 0$, there are net fingers for all the diffusion coefficients $D = 0$, 0.005, 0.01, and 0.02. For the higher diffusion coefficients, the fingers are bigger since they spread the chemical forward and the cells move after it. In contrast, for $D = 0$, the fingers appear not to continue their forward motion but instead, join other fingers. For $\gamma = 0$, there are fingers for all the diffusion coefficients $D = 0$, 0.005, 0.01, and 0.02. Again at $D = 0$, the fingers do not continue their forward motion but instead join other fingers. In the case of higher diffusion coefficients, the fingers move forward slowly since the chemical diffuses to the wounded region, decays, and cannot attract any more cells to go forward. For $\gamma = 50$, there are fingers only for the low diffusion coefficients $D = 0$ and 0.005, whereas for the higher diffusion coefficients, the fingers do not manage to develop, as the chemical diffuses into the wounded region. When the cells begin to move, it is already too late: the chemical has decayed and no longer exists. For $\gamma = 100$, there are fingers for $D = 0$. For the higher diffusion coefficients, the fingers do not manage to develop, as in the case of $\gamma = 50$. In this case for $D = 0$, the fingers are sharp and do not join one another; due to the high decay rate, they are not able to send chemical signals to each other.

The simulation is stochastic, and using the same parameters the results obtained are not exactly the same. This is evident in Fig. 7: four simulations with the same parameters show different results. In the experiment of Poujade et al. (6), many strips of cells were cultured, also resulting in stochastic behavior of the front. To check the general pattern that repeats itself, we investigated the fingering morphology after 1800 MCS without proliferation by performing 30 simulations with the same parameters. Using this set of simulations, we calculated the correlation between two different points of the front as

$$\begin{aligned} &z(x) \text{ (front position at } x) \\ &\hat{z}(x) = z(x) - \langle z(x) \rangle_x \text{ (front position at } x; \\ &\qquad \text{the average front position)}, \end{aligned} \tag{15}$$

$$\langle z(x) \rangle_x = \frac{1}{L_x} \int_0^{L_x} z(x) dx, \tag{16}$$

$$\Gamma_1(\Delta x) = \frac{\int_0^{L_x} \hat{z}(x) \times \hat{z}(x + \Delta x) dx}{\int_0^{L_x} (\hat{z}(x))^2 dx}, \tag{17}$$

where $\Gamma_1(\Delta x)$ is the correlation between two points with distance Δx.

Fig. 8 shows the two-point correlation for 30 simulations. It is apparent that no general pattern exists. To get a typical cell length, an instability analysis with deterministic

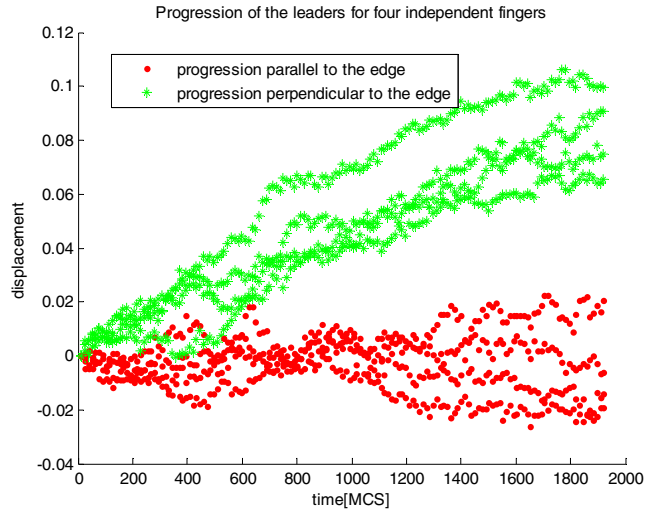

FIGURE 5 Progression of the leaders for four independent fingers. Leaders progress mostly perpendicularly to the initial edge at a constant velocity. $D = 0.005$; $\gamma = 50$.

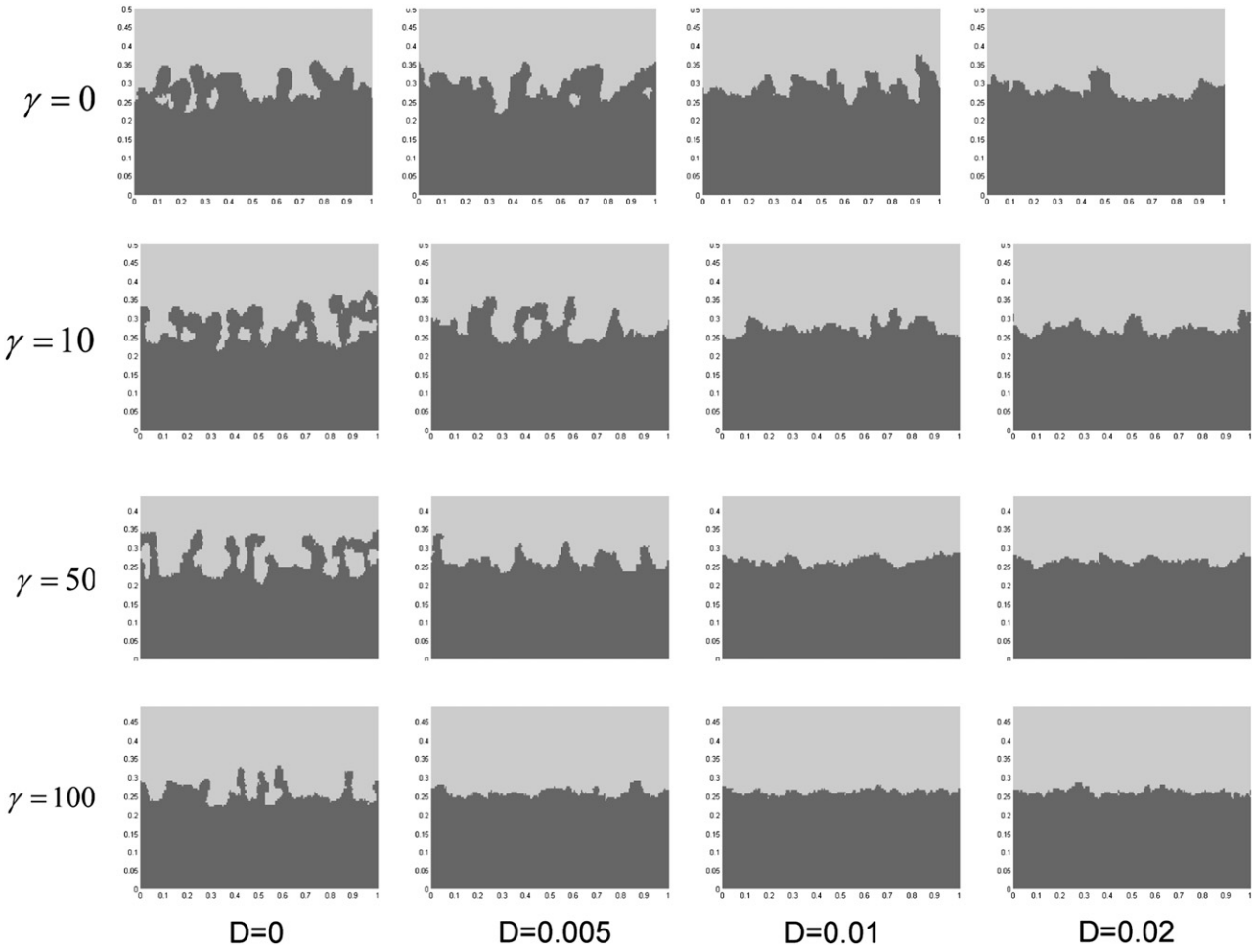

FIGURE 6 Fingering morphology for different D and γ. $t = 1200$ MCS. The diffusion coefficient and the decay rate clearly influence on the fingering morphology: the upper triangular matrix exhibits a fingering morphology, but the rest do not.

equations may be performed. However, it is debatable whether the fingering generation is a dynamic instability-driven process or a continuous evolution of the system, as was shown in the case of the vortex breakdown in confined swirling flows (37).

These simulation results are biologically plausible. Poujade et al. (6), Nikolie et al. (8), and Farooqui and Fenteany (9) encountered a fingering morphology; Grasso et al. (10) found holes close to the front and fingers can obviously be seen. Moreover, the front cells spread their area, as mentioned in Poujade et al. (6) and Farooqui and Fenteany (9). In addition, the velocity of cells gradually increases as they move closer to the wound (8,9) and the cell movement shows a high coordination (8). For low cohesion between cells (due to a decrease in the chemical energy), some cells in the front move forward so fast that they break the continuity of the tissue and holes appear. Increasing the proliferation rate or decreasing the chemotaxis may make these holes disappear. In these experimental studies (6,9,10), the speculated possibilities that cells secrete chemical signals

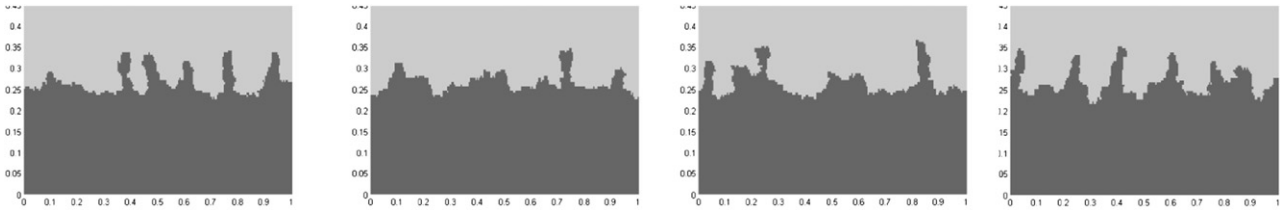

FIGURE 7 Stochastic front behavior: for the same biophysical parameters and the same initial conditions, the cell dynamics and the final fingering morphology are different. $t = 1800$ MCS; $D = 0.005$; decay rate = 50.

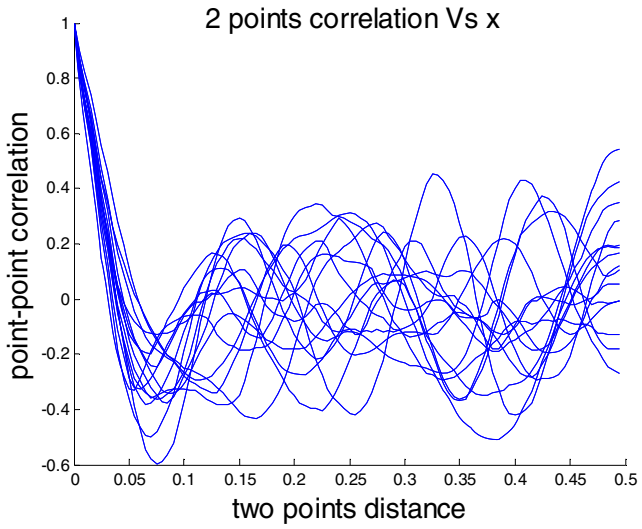

FIGURE 8 Correlation between two front points with distance Δx: no general pattern can be deduced as the results are stochastic. $D = 0.005$; decay rate = 50.

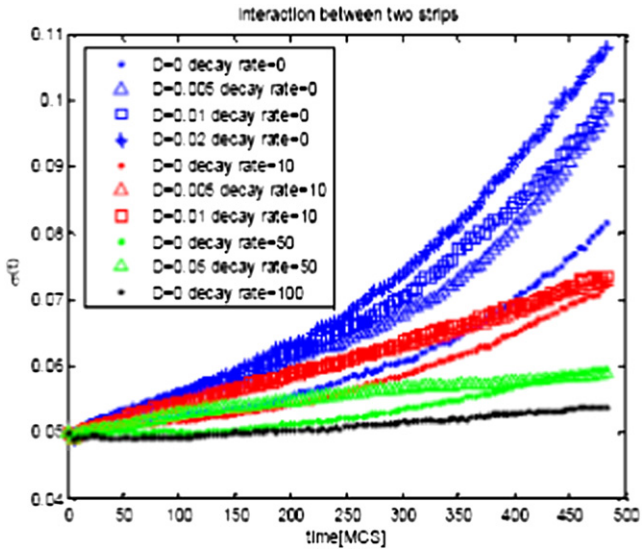

FIGURE 9 Front-front interaction as function of time: two fronts attract each other via chemical signals. The interaction is higher for higher diffusion coefficients and lower decay rates.

or ECM factors to initiate motility are mentioned, but are neither proved nor disproved by experimental results.

Interaction between two strips of cells

Investigating one strip is advantageous for decoupling the effects of its interaction with the counter front. Investigating the possible interaction between two fronts is interesting since when a wound contracts, two opposite borders progressing toward one another rejoin and contract the wound. We show the possible interaction between the two fronts as they progress toward each other. The process is still decoupled from proliferation.

The previous section investigated the fingering morphology generation of one strip for different diffusion coefficients and different decay rates. The decay rate and the diffusion coefficient also play an important role in the possible chemical signaling between two strips of cells. For a certain distance, under different values of diffusion coefficients and decay rates, two strips may communicate or not. However, it should be noted that the stochastic behavior of the cells may overcome this interaction between two strips of cells. To investigate the attraction between two fronts, we define

$$\sigma(t) = 1/\sum_{i} |z_1(x_i, t) - z_2(x_i, t)|, \qquad (18)$$

where $\sigma(t) = 1/$ is the sum of the distances between two fronts at time t. We performed simulations for the same parameters as those in the upper triangle of Fig. 6, where fingers appear. For each of these combinations of parameters, four simulations were run and the average σ was calculated, as can be seen in Fig. 9. Fig. 9 shows that the diffusion coefficient and the decay rate influence the attraction between two fronts. As the decay rate increases, the interaction between the two fronts decreases, and as the coefficient of diffusion increases, the interaction increases.

Increasing the diffusion coefficient enhances the chemical signaling between the two strips of cells and increases the attraction and the correlation between these two strips, whereas the decay rate annihilates the chemical signal between the two strips of cells and there is no coordination and attraction between the two strips. This is biologically plausible, as Gov (7) points out in the experiments done by Poujade et al. (6): the fingers of the two fronts meet themselves and may send chemical signals. This correlation can also be observed in Fig. 10.

Stochastic cells flow

As in the experiment of Poujade et al. (6), and Haga et al. (3), cell flow exhibits interesting patterns. Multicell movement coordination during wound healing results in complex flow. Fig. 11 shows the evolution of one strip that is able to flow in its two free directions. In this figure, the stars indicate the cell mass center position, and the arrows in red show the cell mass center positions in the next 300 MCS. Due to cohesive forces, the leader cells drag the rear cells and create fingers. These fingers compete to pull the cell and some cells, due to these competitive forces, do not know which finger to follow and just turn around; moreover, the symmetry is broken. Decreasing the width of one given strip slows down the progression of the fingers due to competition between the fingers of two different fronts pulling the cells. At a certain width, the morphology of the strip may no longer be a rectangle with fingers, but rather has an undefined shape.

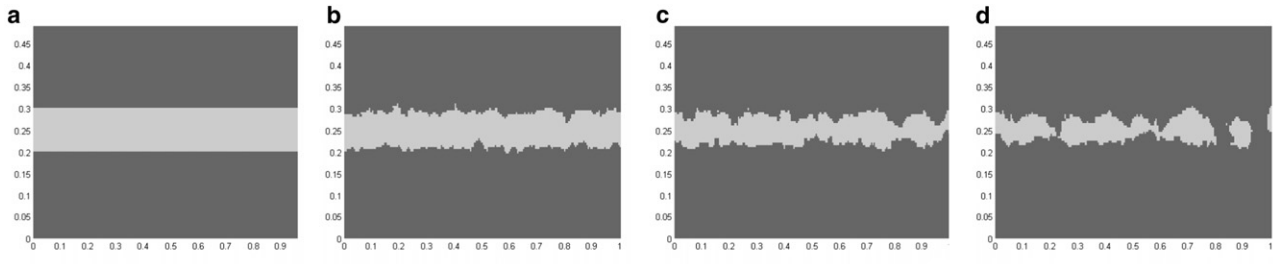

FIGURE 10 During wound healing, two fronts that attract each other and are correlated as fingers send chemical signals and meet. $D = 0.02$, decay rate $= 0$. (*a*) 0 MCS; (*b*) 160 MCS; (*c*) 320 MCS; and (*d*) 480 MCS.

The effect of drift on the chemical is discussed (see the Supporting Material 1) as the effect of a polarized substrate on an initial round geometry (see the Supporting Material 2).

CONCLUSIONS

In this study, we investigated wound healing as a multicell problem in which the effects on cell scale were still able to be examined. We made use of the GGH model with some modifications. We proposed that cells at the border of a wound secrete a chemical that initiates cell motion via chemotaxis. Under this mechanism the front morphology depends on the decay rate and the diffusion coefficient of the diffusive chemical; furthermore, under certain values, fingers develop. These cell fronts are correlated and attracted when running one against another; the cell flow exhibits interesting patterns, such as vortices, and the velocity normal to the front gradually decreases as we move further away from the front.

We also investigated the influence of drift on the chemical, and noted that it may influence the collective cell motion. Moreover, we tested an initial round geometry and the effect of a polarized substrate. It will be interesting to include dynamic proliferation that depends on the cell strain (Supporting Material 3). These results are in accordance with experimental results at the phenomenal level.

The model predicts many results that can be tested experimentally.

Under a certain range of parameters, two fronts progressing against each other are correlated. If this is experimentally corroborated, it will increase the plausibility that cells send chemical signals to orient themselves during epidermal wound healing. However, if the cell fronts are not correlated, this does not disprove the model totally: the diffusion coefficient may be too low or the degradation of the chemical too high to successively send the chemical to its counterpart front.

Furthermore, it is possible to check whether the front-front correlation and the fingering morphology correspond to the predicted front-front correlation and the predicted fingering morphology for some given values of the diffusion coefficient and the decay rate.

Applying a drift to the chemical may influence the collective cell motion as observed (Supporting Material 2). If this is experimentally proven, it will indicate that the cell dynamics is coupled to other chemicals or biological materials. In this case, the experiments may be hard to perform since a drift has been applied such that it does not influence the cells significantly but still drifts the chemical away.

An initial round geometry should be tested experimentally, and the front morphology and dynamics at the cell level should be investigated in this case. Furthermore, it would be

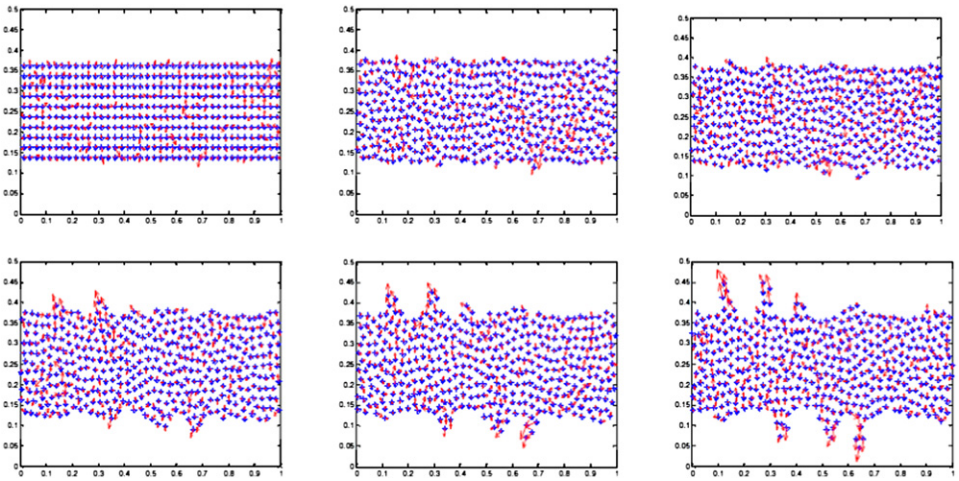

FIGURE 11 Stochastic cells flow: It starts at $t = 0$ MCS and it advances by steps of 300 MCS. Leader cells generate fingers and compete to pull the cells of the submarginal layers. Many cells belong to a particular finger but some are pulled by more than one finger and do not know where to go, and thus simply turn around.

interesting to combine experiments on polarized substrates with different geometries.

These results remain to be checked in the laboratory. New experiments found that in addition to the role of the leader cells in wound repair, traction forces driving collective cell migration arise predominantly many cell rows behind the leading front edge (38). Here, the mathematical model can help offer speculations about plausible mechanisms, which may enhance new experiments to support or disprove the simulation results. Following this, the biological-mathematical modeler should build new models based on the previous experiments. We believe that through such iterative interaction between experimental biologists and biophysicists with mathematical modelers and applied mathematicians, the quantitative understanding of biological processes will be advanced and lead to medical implications.

SUPPORTING MATERIAL

Four figures are available at http://www.biophysj.org/biophysj/supplemental/S0006-3495(09)01196-5.

This research was started while P.Z.B.-Y. was a visiting professor at the Department of Mechanical and Aeronautics Engineering, University of California, San Diego. P.Z.B.-Y. is grateful to Prof. Juan Lasheras for introducing him to this subject. The authors G.Y.O. and P.Z.B.-Y. personally thank the anonymous referees, whose constructive comments helped improve this article.

This research was partially supported by the Samuel and Anne Tolkowsky chair at the Technion-Israel Institute of Technology.

REFERENCES

1. Alamo, J. C., R. Meili, B. Alonso-Latorre, J. Rodriguez, A. Aliseda, et al. 2007. Spatio-temporal analysis of eukaryotic cell motility by improved force cytometry. *Proc. Natl. Acad. Sci. USA.* 104:13343–13348.
2. Lo, C. M., H. B. Wang, M. Dembo, and Y. L. Wang. 2000. Cell movement is guided by the rigidity of the substrate. *Biophys. J.* 79: 144–152.
3. Haga, H., C. Irahara, R. Kobayashi, T. Nakagaki, and K. Kawabata. 2005. Collective movement of epithelial cells on a collagen gel substrate. *Biophys. J.* 88:2250–2256.
4. Larripa, K., and A. Mogilner. 2006. Transport of a 1D viscoelastic actin-myosin strip of gel as a model of a crawling cell. *Physica A.* 372:113–123.
5. Rubinstein, B., K. Jacobson, and A. Mogilner. 2005. Multiscale 2D modeling of a motile simple shaped cell. *SIAM J. MMS.* 3:413–439.
6. Poujade, M., E. Grasland-Mongrain, A. Hertzog, J. Jouanneau, P. Chavrier, et al. 2007. Collective migration of an epithelial monolayer in response to a model wound. *Proc. Natl. Acad. Sci. USA.* 104:15988–15993.
7. Gov, N. S. 2007. Collective cell migration patterns: follow the leader. *Proc. Natl. Acad. Sci. USA.* 104:15970–15971.
8. Nikolie, D. L., A. N. Boettiger, D. Bar-Sagi, J. D. Carbeck, and S. Y. Shvartsman. 2006. Role of boundary conditions in an experimental model of epithelial wound healing. *Am. J. Physiol. Cell Physiol.* 291:C68–C75.
9. Farooqui, R., and G. Fenteany. 2005. Multiple rows of cells behind an epithelial wound edge extend cryptic lamellipodia to collectively drive cell sheet movement. *J. Cell Sci.* 118:51–63.
10. Grasso, I., J. A. Hernandez, and S. Chifflet. 2007. Roles of wound geometry, wound size, and extracellular matrix in the healing response of bovine corneal endothelial cells in culture. *Am. J. Physiol. Cell Physiol.* 293:C1327–C1337.
11. Bindschadler, M., and J. L. McGrath. 2007. Sheet migration by wounded monolayers as an emergent property of single-cell dynamics. *J. Cell Sci.* 120:876–884.
12. Murray, J. D. 2003. Mathematical Biology II: Spatial Models and Biomedical Applications. Springer, New York.
13. Sherratt, J. A., and J. D. Murray. 1991. Mathematical analysis of a basic model for epidermal wound healing. *J. Math. Biol.* 29:389–404.
14. Dale, P. D., P. K. Maini, and J. A. Sherratt. 1994. Mathematical modeling of corneal epithelial wound healing. *Math. Biosci.* 124:127–147.
15. Maini, P. K., D. L. S. McElwain, and D. Leavesley. 2004. Traveling waves in a wound healing assay. *Appl. Math. Lett.* 17:575–580.
16. Maini, P. K., D. L. S. McElwain, and D. Leavesley. 2004. Traveling wave model to interpret a wound-healing cell migration assay for human peritoneal mesothelial cells. *Tissue Eng.* 10:475–482.
17. Cai, A. Q., K. A. Landman, and B. D. Hughes. 2007. Multi-scale modeling of a wound-healing cell migration assay. *J. Theor. Biol.* 245:576–594.
18. Graner, F., and J. A. Glazier. 1992. Simulation of biological cell sorting using a two-dimensional extended Potts model. *Phys. Rev. Lett.* 69:2013–2016.
19. Savill, N. J., and P. Hogeweg. 1997. Modeling morphogenesis: from single cells to crawling slugs. *J. Theor. Biol.* 184:229–235.
20. Turner, S., and J. A. Sherratt. 2002. Intercellular adhesion and cancer invasion: a discrete simulation using the extended Potts model. *J. Theor. Biol.* 216:85–100.
21. Popalawski, N. J., A. Shirinifard, M. Swat, and J. A. Glazier. 2008. Simulation of single-species bacterial-biofilm growth using the Glazier-Graner-Hogeweg model and the Compucell 3D modeling environment mathematical biosciences. *Math. Biosci. Eng.* 5:355–388.
22. Ouchia, N. B., J. A. Glazier, J. P. Rieu, A. Upadhyaya, and Y. Sawada. 2003. Improving the realism of the cellular Potts model in simulations of biological cells. *Physica A.* 329:451–458.
23. Turner, S., J. A. Sherratt, and K. J. Painter. 2004. From a discrete to a continuous model of biological cell movement. *Phys. Rev. E.* 69:021910.
24. Alber, M. S., N. Chen, T. Glimm, and P. M. Lushnikov. 2006. Multiscale dynamics of biological cells with chemotactic interactions: from a discrete stochastic model to a continuous description. *Phys. Rev. E.* 73:051901.
25. Alber, M. S., N. Chen, P. M. Lushnikov, and S. A. Newman. 2007. Continuous macroscopic limit of a discrete stochastic model for interaction of living cells. *Phys. Rev. Lett.* 99:168102.
26. Izaguirre, J. A., R. Chaturvedi, C. Huang, T. Cickovski, J. Coffland, et al. 2004. Compucell, a multi-model framework for simulation of morphogenesis. *Bioinformatics.* 20:1129–1137.
27. Cickovski, T. M., C. Huang, R. Chaturvedi, T. Glimm, H. G. E. Hentschel, et al. 2005. A framework for three-dimensional simulation of morphogenesis. *Trans. Comp. Biol. Bioinform.* 2:273–288.
28. Bao, G., and S. Surech. 2003. Cell and molecular mechanics of biological materials. *Nat. Mater.* 2:715–725.
29. Kittel, C., and H. Kroemer. 1980. Thermal Physics. W. H. Freeman and Company, New York.
30. Metropolis, N., A. W. Rosenbluth, M. N. Rosenbluth, A. H. Teller, and E. Teller. 1951. Equation of state calculations by fast computing machines. *J. Chem. Phys.* 21:1087–1092.
31. Balter, A., R. M. H. Merks, N. J. Popalawski, M. Swat, and J. Glazier. 2007. The Glazier-Graner-Hogeweg model: extensions, future directions, and opportunities for further study. *In* Single Cell-Based Model in Biology and Medicine. A. R. A. Anderson, M. A. J. Chaplain, and K. J. Rejniak, editors. Birkhäuser, Springer, New York. 151.
32. Popalawski, N. J. 2005. Volume and surface constraints in the cellular Potts model. ArXiv:physics/0512129.

33. Shlomovitz, R., and N. S. Gov. 2008. Curved inclusions surf membrane waves. *Europhys. Lett.* 84:58008.

34. Kessler, D. A., and H. Levine. 1993. Pattern formation in *Dictyostelium* via the dynamics of cooperative biological entities. *Phys. Rev. E.* 48:4801–4804.

35. Jiang, Y., H. Levine, and J. Glazier. 1998. Possible cooperation of differential adhesion and chemotaxis in mound formation of *Dictyostelium*. *Biophys. J.* 75:2615–2625.

36. Philip, E. P. 2000. Stochastic Integration and Differential Equations. Springer, New York.

37. Gelfat, A. Y., P. Z. Bar-Yoseph, and A. Solan. 1996. Stability of confined swirling flow with and without vortex breakdown. *J. Fluid Mech.* 311:1–36.

38. Trepat, X., M. R. Wasserman, T. E. Angelini, E. Millet, D. A. Weitz, et al. 2009. Physical forces during collective cell migration. *Nat. Phys.* 10.1038/NPHYS1269.